

## Magnetic zinc oxide/silica microbeads for the photocatalytic degradation of azo dyes

Mohammed Al-Sharabi<sup>a</sup>, Daniele Baiocco<sup>b</sup>, Benjamin T. Lobel<sup>c</sup>, Olivier J. Cayre<sup>c</sup>, Zhibing Zhang<sup>b</sup>, Alexander F. Routh<sup>a,\*</sup>

<sup>a</sup> Department of Chemical Engineering and Biotechnology, University of Cambridge, Cambridge CB3 0AS, UK

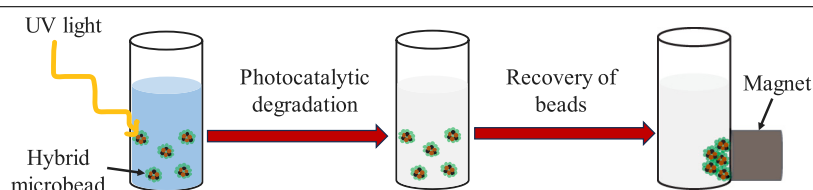
<sup>b</sup> School of Chemical Engineering, University of Birmingham, Birmingham B15 2TT, UK

<sup>c</sup> School of Chemical and Process Engineering, University of Leeds, Leeds LS2 9JT, UK

### HIGHLIGHTS

- A new photocatalyst in the form of ZnO/Fe<sub>3</sub>O<sub>4</sub>/SiO<sub>2</sub> hybrid microbeads was fabricated for the photocatalytic degradation of methylene blue.
- The hybrid microbeads performed better than ZnO powder at the same conditions due to higher adsorption and degradation.
- Higher degradation is observed with decreasing initial dye concentration and increasing catalyst dosage.
- Full recovery of the hybrid microbeads for further degradation experiments was achieved due to the presence of magnetic nanoparticles within the beads.

### GRAPHICAL ABSTRACT



### ARTICLE INFO

#### Keywords:

Magnetic zinc oxide/silica microbeads  
Nanoparticles  
Azo dyes  
Methylene blue  
Photocatalytic degradation  
Wastewater treatment

### ABSTRACT

Photocatalysis is a promising technique for the complete degradation of azo dyes that are present in wastewater. In this work, a new photocatalyst in the form of ZnO/Fe<sub>3</sub>O<sub>4</sub>/SiO<sub>2</sub> hybrid microbeads was fabricated for the photocatalytic degradation of methylene blue. The microbeads were synthesised through self-assembly and subsequent agglomeration of nanoparticles within an aqueous phase of a water-in-oil emulsion template. Photocatalytic degradation experiments were conducted through exposure of a methylene blue solution to UV light. The hybrid microbeads performed better than ZnO powder at the same initial dye and ZnO concentration because of higher adsorption and degradation. The initial concentration of dye solution and catalyst dosage have a significant impact on the degradation. Higher degradation is seen with lower initial dye concentration and higher catalyst dosage. The presence of magnetic nanoparticles within the beads allows for their full recovery and reuse for degradation experiments. Complete degradation of dye was achieved using the new ZnO/Fe<sub>3</sub>O<sub>4</sub>/SiO<sub>2</sub> microbeads.

\* Corresponding author.

E-mail address: [afr10@cam.ac.uk](mailto:afr10@cam.ac.uk) (A.F. Routh).

<https://doi.org/10.1016/j.colsurfa.2024.134169>

Received 26 February 2024; Received in revised form 18 April 2024; Accepted 30 April 2024

Available online 9 May 2024

0927-7757/© 2024 The Author(s). Published by Elsevier B.V. This is an open access article under the CC BY license (<http://creativecommons.org/licenses/by/4.0/>).

## 1. Introduction

Synthetic organic dyes, such as azo dyes, are widely used in the manufacture of pharmaceuticals, foods, cosmetics, textiles, leather and paper products [1–3]. Azo dyes are synthetic organic compounds that contain one or more azo ( $-N=N-$ ) groups in their molecular structures [4]. The discharge of industrial effluents contaminated with azo dyes into water bodies adversely impacts the environment and human health [5,6]. The high water solubility and the long-term thermal and photostabilities of azo dyes make their removal from industrial effluents challenging [7]. An example of an azo dye is methylene blue (MB), which is cationic and commonly used in the textile industry for colouring textiles, such as cotton, silk and wool [8,9]. The presence of MB in wastewater has long-term adverse impacts on the aquatic environment since the dye blocks sunlight from accessing water bodies, which in turn inhibits the photosynthetic activity of aquatic life [10, 11]. Furthermore, prolonged human exposure to MB can cause a number of health issues, such as shortness of breath, eye and skin irritation, nausea, rapid heartbeat and mental confusion [12]. Therefore, it is desirable to completely remove dye pollutants from wastewater.

Various physical, chemical and biological methods, such as membrane filtration, adsorption, coagulation–flocculation, chlorination, ozonation, ion exchange, electrochemical oxidation and biodegradation have been used for the removal of azo dyes from wastewater [13–15]. However, these techniques have some drawbacks, such as high operational costs, high energy consumption, generation of secondary pollutants during treatment and low efficiency of dye removal due to the chemical stability and complex aromatic structures [16–18]. Photocatalysis is a promising method for the degradation of azo dyes through mineralisation into water, carbon dioxide and mineral acids without producing secondary pollutants [19]. For instance, metal oxide semiconductors, such as titanium dioxide ( $TiO_2$ ) [20,21], zinc oxide (ZnO) [22–25] and tin oxide ( $SnO_2$ ) [26,27] have been used as photocatalysts for the degradation of MB. ZnO has been widely adopted as a photocatalyst due to its wide energy band-gap (3.37 eV) and large excitation binding energy (60 meV) at room temperature, non-toxicity, biocompatibility, excellent physical and chemical stability and low cost [28–30]. In addition, the insolubility of ZnO in water [31] and its capability of completely degrading a number of azo dyes [32,33] make it a good candidate for the removal of dye pollutants.

Hybridisation is considered an effective technique for enhancing the photocatalytic performance of a photocatalyst [34–37]. A range of different materials, such as semiconductors, noble metals, transition metals and carbon have been used to enhance the photocatalytic performance of ZnO [38–40]. Recently, graphene oxide (GO) and reduced graphene oxide (rGO) have been incorporated in the design of ZnO-based photocatalysts to improve the degradation of MB. Examples include ZnO@GO [41], ZnO–rGO [42] and rGO/ $TiO_2$ /ZnO nanocomposites [43]. Graphene acts as an electron transport facilitator for the transfer and separation of the photogenerated electrons [44]. Furthermore, coupling ZnO with magnetic nanoparticles to form magnetic nanocomposites allows for easy recovery of the nanocomposites from the treated dye solution [45]. Harraz et al. [46] synthesised magnetically responsive photocatalysts, i.e. titania-silica/cobalt ferrite ( $TiO_2$ – $SiO_2$ /CoFe $_2$ O $_4$ ) nanocomposites, for the efficient and easy separation of the photocatalyst from a treated MB solution, allowing for recyclability and reusability. Iron oxide (Fe $_3$ O $_4$ ) has attracted significant attention due to its magnetic characteristics, low toxicity and biocompatibility [47]. Recently, Thi Lan Huong et al. [48] fabricated magnetically separable ZnO/Fe $_3$ O $_4$  nanocomposites by a facile hydrothermal technique to enhance the degradation efficiency of MB under both UV and visible light irradiation. The higher degradation efficiency using ZnO/Fe $_3$ O $_4$  nanocomposites compared to ZnO nanoparticles can be attributed to the transfer of electrons from the conduction band of ZnO to that of Fe $_3$ O $_4$  and/or from the conduction band of Fe $_3$ O $_4$  to new defect states in ZnO. Several studies have

also reported on similar systems consisting of magnetically separable photocatalysts comprising of ZnO and Fe $_3$ O $_4$  for the degradation of MB [49,50]. In related work, Brossault et al. [51] synthesised a magnetic photocatalyst in the form of  $TiO_2$ /Fe $_3$ O $_4$ /SiO $_2$  microbeads for the degradation of MB. The composite microbeads were prepared in a simple, cost-effective, efficient and environmentally-friendly approach at room temperature through the salt-induced destabilisation of nanoparticles in a water-in-oil (W/O) emulsion template.

This work reports fabrication of a new photocatalyst in the form of ZnO/Fe $_3$ O $_4$ /SiO $_2$  composite microbeads, based on the production method reported by Brossault et al. [51]. This method is fast, cost-effective and does not involve the use of hazardous chemicals, which makes it a promising approach for the preparation of magnetically separable composite microbeads consisting of a range of different photocatalysts for wastewater treatment applications. It has been found that ZnO has higher quantum and photocatalytic efficiency in comparison with  $TiO_2$  [52]. Since ZnO and  $TiO_2$  have similar photocatalytic degradation mechanisms [53,54] and comparable band gap energies [55], ZnO is considered as a potential alternative for the photocatalytic degradation of organic dyes. Unlike the work conducted by Brossault et al. [51], the current work considers the adsorption of MB onto the surface of ZnO/Fe $_3$ O $_4$ /SiO $_2$  microbeads prior to performing the photocatalytic degradation experiments. To investigate our novel hybrid microbeads, the effect of a number of parameters, such as the catalyst dosage, initial concentration of MB solution, as well as the porosity of beads was studied. In addition, the recyclability and reusability of the photocatalytic beads were investigated by placing a magnet in contact with an aqueous suspension of ZnO/Fe $_3$ O $_4$ /SiO $_2$  beads and using the recovered beads for further degradation of fresh MB solutions.

## 2. Materials and methods

### 2.1. Materials

An aqueous phase was prepared which consisted of silica particles (Ludox HS-40, 40 wt% suspension in water, Sigma-Aldrich), zinc oxide, ZnO, (nanopowder, <50 nm in diameter, >97% purity, Sigma-Aldrich), iron oxide, Fe $_3$ O $_4$ , (nanopowder, 50–100 nm in diameter, 97% purity, Alfa Aesar) and polyoxyethylenesorbitan mono-laurate (Tween 20, Acros Organics). An oil phase was composed of sunflower oil (Sainsbury's) or a mixture of sunflower oil and sorbitan monooleate (Span 80, Sigma-Aldrich). Calcium chloride dihydrate, CaCl $_2$ ·2H $_2$ O (>99% purity, Acros Organics) was used for destabilisation of the nanoparticles and the subsequent formation of microbeads. Absolute ethanol (99.8% purity, Acros Organics) was utilised for washing the microbeads. Methylene blue hydrate (Sigma-Aldrich) was used as a model dye. All materials were used as received without further purification or modification.

### 2.2. Dynamic light scattering

Dynamic light scattering (DLS) measurements, at an angle of 90°, were conducted using a NanoBrook Omnio system (Brookhaven Instruments) to determine the mean diameter of silica nanoparticles. 4 mL of an aqueous colloidal dispersion was added to a plastic cuvette, which was then placed in the chamber of the DLS equipment. The mean particle size was obtained by averaging three measurements per sample. Each measurement was performed at 20 °C and neutral pH, with a duration of 120 s and an equilibrium time of 60 s.

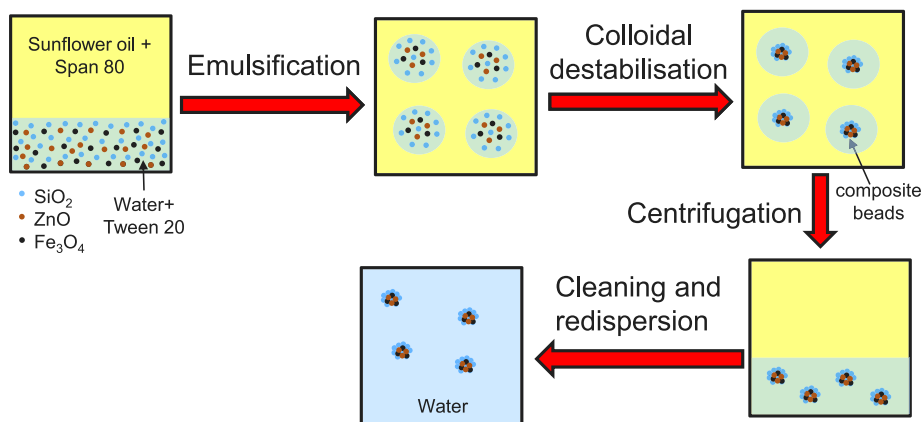


Fig. 1. The preparation method of ZnO/Fe<sub>3</sub>O<sub>4</sub>/SiO<sub>2</sub> microbeads through the salt-induced destabilisation of nanoparticles in a W/O emulsion template.

### 2.3. Preparation of the magnetic photocatalytic microbeads

The ZnO/Fe<sub>3</sub>O<sub>4</sub>/SiO<sub>2</sub> microbeads were prepared by self-assembly and agglomeration of nanoparticles within the aqueous phase of a W/O emulsion template, as illustrated in Fig. 1. Silicon dioxide (30 wt%), zinc oxide (5 wt%), iron oxide (5 wt%) and Tween 20 (1 wt%) were mixed for 1 min using an ultrasonic homogeniser (FB-120 Sonic Dismembrator equipped with a Model CL-18 probe, Fisher Scientific) to prepare the aqueous phase. The oil phase was pure sunflower oil or a mixture of sunflower oil with 1 wt% of Span 80. The W/O emulsion was produced by adding 1 g of the aqueous phase dropwise to 99 g of the oil phase and stirring the mixture at 5000 rpm for 1 min using a Silverson mixer (model SL2). The stirring speed was reduced to 3000 rpm and 1 mL of 1 M CaCl<sub>2</sub> aqueous solution was added dropwise to induce the destabilisation and hence agglomeration of nanoparticles into the microbeads. To wash the surface oil off the microbeads, the emulsion was split into three different tubes and centrifuged at 3000 rpm for 5 min (Multifuge 1 S-R, Heraeus). After removal of the oil phase, the microbeads were twice washed using 10 mL of absolute ethanol and centrifuged at 3000 rpm for 5 min. Finally, the clean microbeads were dispersed in 5 mL of deionised water.

### 2.4. Characterisation of microbeads using microscopy

The size and morphology of the beads were investigated by imaging the samples using a bright-field optical microscope (Leica DME) equipped with a 63x objective lens and a scanning electron microscope (SEM, Tescan Mira3 FEG-SEM microscope) operating at an acceleration voltage of 5 kV. ImageJ software was utilised to determine the mean diameter  $\pm$  standard deviation of the microbeads using 200 randomly selected by eye from the SEM images. Transmission electron microscopy (TEM) micrographs were obtained using a Thermo Scientific (FEI Company) Talos F200X G2 microscope equipped with a Ceta 4k  $\times$  4k CMOS camera and operating at an acceleration voltage of 200 kV. Scanning transmission electron microscopy (STEM) images were collected using a Fischione HAADF detector at a camera length of 98 mm and energy-dispersive X-ray spectroscopy (EDX) spectra and maps were obtained using the Super-X EDX detector system which consists of 4 windowless silicon drift detectors. The TEM samples were prepared by pipetting 5  $\mu$ L of an aqueous suspension onto continuous carbon 300 mesh Cu grids.

### 2.5. Zeta potential measurements

Zeta potential measurements were conducted using a NanoBrook Omnio system (Brookhaven Instruments) to determine the surface charge of the ZnO/Fe<sub>3</sub>O<sub>4</sub>/SiO<sub>2</sub> microbeads. 1.25 mL of an aqueous

dispersion of the microbeads at neutral pH was used for the measurements. The average zeta potential was determined based on three measurements per sample. Each measurement was performed at room temperature with 25 cycles.

### 2.6. Photocatalytic degradation experiments

The photocatalytic degradation experiments were performed by exposing the MB solution containing the dispersed photocatalyst to UV light from a 36 W UV lamp source with a wavelength of 365 nm in an enclosure. Prior to exposure, the suspension was kept in the dark for 30 min to establish the adsorption/desorption equilibrium. For each degradation experiment, a specific amount of the photocatalyst was added to a fixed volume of 50 mL of an aqueous MB solution with a specific initial concentration. The photoreaction was conducted at room temperature with continuous stirring. 5 mL of the sample was collected at different times up to 120 min, and then centrifuged at 10000 rpm for 5 min. The absorbance of the supernatant liquid contained within a 1 cm pathlength cuvette was measured using a UV-Vis spectrometer (Cary 60, Agilent Technologies) and the value of the maximum absorbance in the wavelength range of 400 to 800 nm was used to calculate the corresponding concentration. The effect of the photocatalyst dosage on the degradation of MB was investigated by dispersing different amounts of the ZnO/Fe<sub>3</sub>O<sub>4</sub>/SiO<sub>2</sub> beads (20, 30 and 40 mg), corresponding to 2.5, 3.75 and 5 mg of ZnO nanopowder, in a MB solution with an initial concentration of 10 mg L<sup>-1</sup>. A fixed dosage of the ZnO/Fe<sub>3</sub>O<sub>4</sub>/SiO<sub>2</sub> beads (20 mg), corresponding to 2.5 mg of ZnO nanopowder, was added to three different initial concentrations of MB (1, 5 and 10 mg L<sup>-1</sup>) to study the impact of initial dye concentration. The effect of the bead porosity was investigated by comparing the photocatalytic performance of 20 and 40 mg of ZnO/Fe<sub>3</sub>O<sub>4</sub>/SiO<sub>2</sub> beads that were prepared with and without Span 80 using a MB solution with an initial concentration of 10 mg L<sup>-1</sup>.

### 2.7. Magnetic recovery and reusability of microbeads

The magnetic response of the ZnO/Fe<sub>3</sub>O<sub>4</sub>/SiO<sub>2</sub> beads was tested by applying an external magnetic field using a 20  $\times$  20 mm rare-earth neodymium magnet (e-Magnets UK) to a 5 mL aqueous suspension of beads. Reusability studies were conducted through the magnetic recovery of the ZnO/Fe<sub>3</sub>O<sub>4</sub>/SiO<sub>2</sub> beads and their redispersion in 50 mL of fresh MB solution with an initial concentration of 10 mg L<sup>-1</sup>. Two further repeats were performed to study the reusability of the ZnO/Fe<sub>3</sub>O<sub>4</sub>/SiO<sub>2</sub> beads.

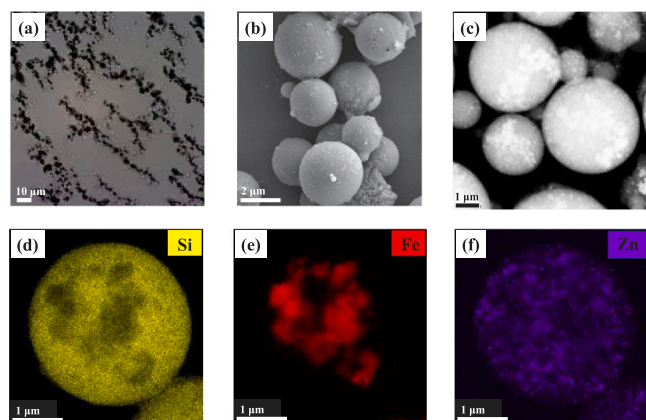


Fig. 2. Images of the ZnO/Fe<sub>3</sub>O<sub>4</sub>/SiO<sub>2</sub> microbeads without Span 80 that were acquired by (a) bright-field optical microscopy (b) SEM (c) STEM and (d, e, f) EDX analysis.

### 3. Results and discussion

#### 3.1. Morphology of microbeads

It can be seen from the bright-field optical micrograph, SEM and STEM images in Fig. 2 that spherical ZnO/Fe<sub>3</sub>O<sub>4</sub>/SiO<sub>2</sub> microbeads were successfully prepared through the CaCl<sub>2</sub>-induced destabilisation and subsequent agglomeration of nanoparticles in a W/O emulsion template in the absence of Span 80. Black regions within the microbeads are observed in the bright-field optical microscopy image (Fig. 2a), which suggests the presence of Fe<sub>3</sub>O<sub>4</sub> nanoparticles in the bead structure. Similar results were observed by Brossault et al. [51] for the TiO<sub>2</sub>/Fe<sub>3</sub>O<sub>4</sub>/SiO<sub>2</sub> beads. Fig. 2a also shows that the ZnO/Fe<sub>3</sub>O<sub>4</sub>/SiO<sub>2</sub> beads appear to be aligned, which can be attributed to the attraction between the magnetic Fe<sub>3</sub>O<sub>4</sub> components. The SEM image (Fig. 2b) shows that the beads have a smooth surface structure. The STEM image (Fig. 2c) also shows the smoothness of the bead's structure and confirms the presence of different nanoparticles within the beads as evident from the contrast in transmitted light intensity across the bead. EDX analysis (Fig. 2d-f) was performed to obtain the elemental mapping of the different constituent nanoparticles within the beads, i.e. silica, ZnO and Fe<sub>3</sub>O<sub>4</sub> nanoparticles. The EDX results confirm the presence of all the constituent nanoparticles within the microbeads. The silica and ZnO nanoparticles are homogeneously distributed within the beads, unlike the Fe<sub>3</sub>O<sub>4</sub> nanoparticles which appear more clustered. The low homogeneity of the Fe<sub>3</sub>O<sub>4</sub> nanoparticles distribution can be attributed to the strong attraction between the Fe<sub>3</sub>O<sub>4</sub> nanoparticles due to their magnetic property. This is similar to observations made by Brossault et al. [51] for TiO<sub>2</sub>/Fe<sub>3</sub>O<sub>4</sub>/SiO<sub>2</sub> beads.

Span 80 was added to the oil phase of the W/O emulsion to modify the porosity of beads. The resulting impact on the photocatalytic degradation of MB was then investigated. The SEM and TEM images (Fig. 3) show that the beads prepared with 1 wt% of Span 80 have a rougher and more porous structure. Brossault and Routh [56] demonstrated that the addition of Span 80 to the oil phase resulted in the production of silica microbeads with a more porous structure and that the bead porosity increases with increasing the concentration of Span 80. This was explained by two possible mechanisms: the adsorption of oil onto the surface of silica nanoparticles via Span 80 within the formed beads, which is then removed during the washing process leaving gaps in the clean beads (ii) the steric hindrance preventing the packing of silica nanoparticles due to the formation of micellar structures at the surface of particles. Similar observations were reported for the silica beads containing other functional nanoparticles, e.g. Fe<sub>3</sub>O<sub>4</sub>/SiO<sub>2</sub> [56] and TiO<sub>2</sub>/Fe<sub>3</sub>O<sub>4</sub>/SiO<sub>2</sub> microbeads [51], where the beads prepared without Span 80 had a relatively smooth structure

with no or very small porosity. The TEM images also show that the ZnO/Fe<sub>3</sub>O<sub>4</sub>/SiO<sub>2</sub> microbeads have a composite structure consisting of agglomerated constituent nanoparticles. Fig. 3 also shows the size distributions of the ZnO/Fe<sub>3</sub>O<sub>4</sub>/SiO<sub>2</sub> microbeads based on the SEM images. The size distribution results show that Span 80 has negligible effect on the size distribution. The beads without Span 80 have an average diameter of  $2.53 \pm 0.78 \mu\text{m}$ , and the beads prepared with 1 wt% of Span 80 have an average diameter of  $2.57 \pm 0.67 \mu\text{m}$ . The size distribution values are presented as mean  $\pm$  standard deviation.

#### 3.2. Analysis of UV-Vis spectra of ZnO and MB

Fig. 4 shows the UV-Vis absorption spectra of an aqueous dispersion of ZnO powder ( $100 \text{ mg L}^{-1}$ ) and an aqueous MB solution ( $5 \text{ mg L}^{-1}$ ) over a wavelength range of 220 to 800 nm. It can be seen that ZnO has an absorption peak at 368 nm. Previous studies have reported on absorption peaks of ZnO nanoparticles between 360 to 372 nm [22,57], which is similar to the recorded value in this work. Furthermore, Fig. 4 shows that MB has absorption peaks at 246, 292, 610 and 664 nm, which are consistent with the values reported by Dinh et al. [58]. The absorption peak at 664 nm was tracked to determine dye removal during photocatalytic degradation upon exposure to UV light. This absorption peak was selected as it is located far away from the absorption peak of ZnO. It was ensured that the MB solution, collected at different intervals during the photocatalytic degradation experiments, did not contain any photocatalyst particles through ensuring the absence of the absorption peak of ZnO.

The band gap energy,  $E_g$ , of the ZnO nanoparticles in electron volts (eV) corresponds to their absorption limit and can be determined using Eq. (1) [59]

$$E_g = \frac{1240}{\lambda} \quad (1)$$

where  $\lambda$  is the wavelength at which the maximum absorption is obtained in (nm).  $E_g$  of the ZnO photocatalysts powder was calculated to be 3.37 eV, which is in agreement with literature [29,60].

#### 3.3. Photocatalytic degradation

The mechanism of the photocatalytic degradation of MB using ZnO under UV light is illustrated in Fig. 5. The exposure of ZnO to UV light with photonic energy ( $h\nu$ ) that is equal to or greater than the band gap energy of ZnO, i.e.  $h\nu \geq E_g$ , results in the excitation of electrons from the valence band (VB) to the conduction band (CB) [61]. The photoexcitation process generates electron-hole ( $e^-/h^+$ ) pairs (Eq. (2)), which can migrate to the surface of ZnO to be used in the redox reactions, which involve the reaction of  $h^+$  with water and hydroxide ions to generate hydroxyl radicals as well as the reaction of  $e^-$  with oxygen to generate super oxide radical anions and hence hydrogen peroxide (Eqs. (3)–(7)). The hydroxyl radicals produced from the reaction of hydrogen peroxide with superoxide radicals (Eqs. (8)–(10)) are potent oxidising agents, which interact with the MB dye adsorbed on the ZnO surface to generate intermediates and products, such as H<sub>2</sub>O, CO<sub>2</sub> and mineral acids (Eqs. (11) and (12)) [61].



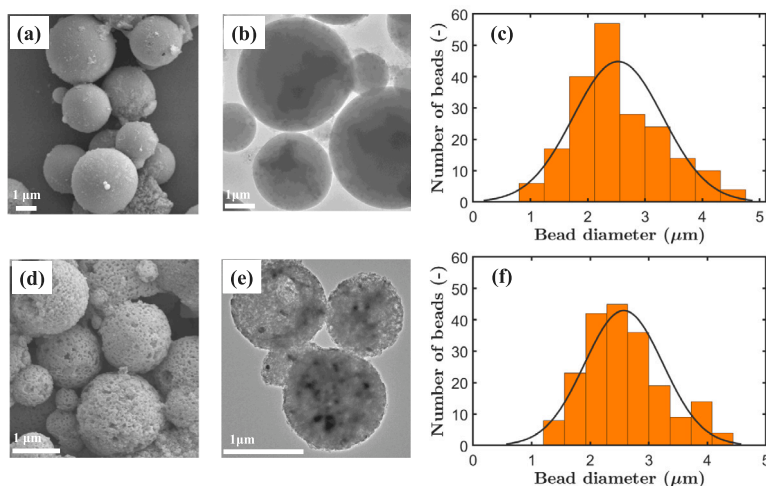


Fig. 3. SEM (a, d) and TEM (b, e) images and the corresponding size distributions fitted with a normal density function as a solid black curve (c, f) of the ZnO/Fe<sub>3</sub>O<sub>4</sub>/SiO<sub>2</sub> microbeads without Span 80 (top) and with 1 wt% Span 80 (bottom).

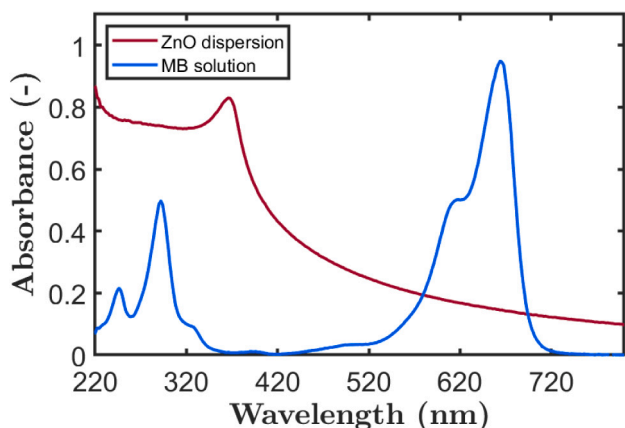


Fig. 4. UV-Vis absorbance spectra of aqueous dispersion of ZnO powder (100 mg L<sup>-1</sup>) and MB solution (5 mg L<sup>-1</sup>). A photonic energy equal to or greater than 3.37 eV (i.e. at a wavelength below 368 nm) is required for the excitation of ZnO.

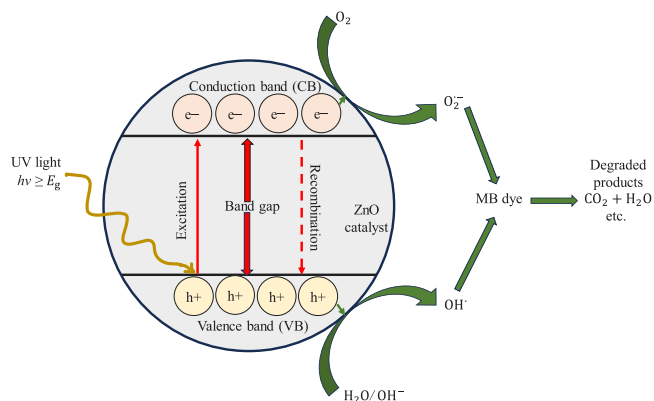


Fig. 5. The mechanism of the photocatalytic degradation of MB dye by ZnO under UV light.

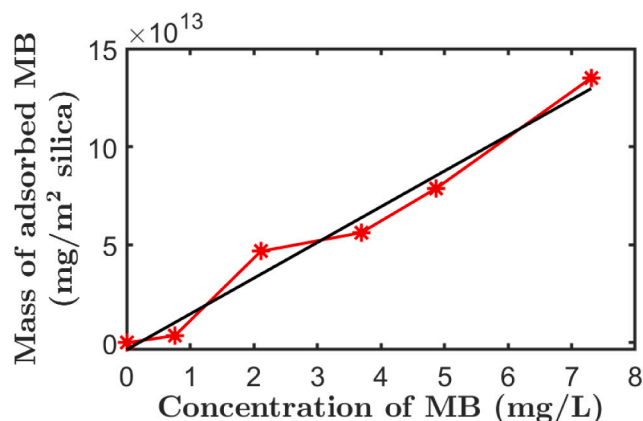
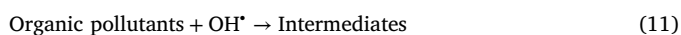


Fig. 6. Adsorption isotherm showing the amount of MB adsorbed onto the surface of silica nanoparticles as a function of the final concentration of MB at 20 °C. Each data point is a single measurement. The adsorption measurement was conducted by adding 15 mg of silica nanoparticles to 50 mL of MB solution with varying concentrations and leaving the dispersion in the dark for 30 min. The size, i.e. mean diameter, of silica nanoparticles determined using dynamic light scattering is 20 ± 1 nm (mean ± standard deviation). The black line represents a linear fit of the data points.

Prior to performing the photocatalytic degradation, it is crucial to investigate the adsorption of dye molecules from an aqueous solution onto the surface of ZnO as the photocatalytic degradation of MB mainly occurs on the surface [62]. Therefore, the MB solution containing the dispersed photocatalyst was kept in the dark for 30 min to establish the adsorption/desorption equilibrium. Fig. 6 shows the amount of MB adsorbed onto the surface of silica nanoparticles, as calculated in Appendix A.1. It can be seen that the mass of MB adsorbed onto the surface of silica nanoparticles increases with increasing the concentration of MB. Furthermore, photolysis experiments were conducted and it was found that the change in the initial concentration of MB (1, 5 and 10 mg L<sup>-1</sup>) upon exposure to UV light for 120 min was negligible, which indicates that MB does not significantly photodecompose in the absence of photocatalyst at these conditions.

Fig. 7 shows the change in the UV-Vis absorption spectra of MB during the photocatalytic degradation of a MB solution with an initial dye concentration of 5 mg L<sup>-1</sup> by 2.5 mg of ZnO powder and its equivalent amount in 20 mg of ZnO/Fe<sub>3</sub>O<sub>4</sub>/SiO<sub>2</sub> beads. It can be seen from Fig. 7 that the initial dye concentration of MB decreases significantly after keeping the dispersion of MB and beads in the dark for 30 min

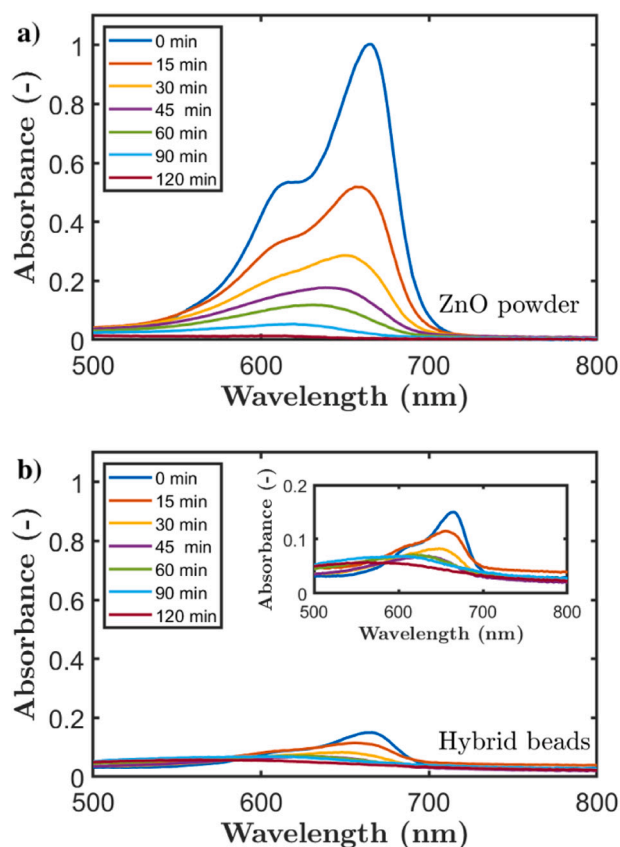


Fig. 7. The UV-Vis absorption spectra of the photocatalytic degradation of a MB solution with an initial dye concentration of  $5 \text{ mg L}^{-1}$  using (a) ZnO powder (2.5 mg) and (b) its equivalent amount in 20 mg ZnO/Fe<sub>3</sub>O<sub>4</sub>/SiO<sub>2</sub> beads. The beads were prepared without Span 80. Time was measured from the start of the photocatalytic degradation process.

compared to that of ZnO powder and MB. This can be explained by the high adsorption of the MB molecules onto the surface of beads likely due to an electrostatic interaction. It can also be seen from Fig. 7 that the intensity of the absorption peak at 664 nm gradually decreases, indicating the decomposition of the auxochrome group of MB [63]. The disappearance of this absorption peak indicates the complete degradation of MB, which occurs faster using the beads compared to the ZnO powder. The UV-Vis spectra of MB during the degradation process by ZnO were also investigated in the full range of 220 to 800 nm. Fig. A.13 shows that the peaks at 246, 292 and 610 nm gradually disappear, confirming the decomposition of MB.

### 3.3.1. Effect of initial concentration of MB solution

The amount of MB adsorbed onto the surface of ZnO nanopowder, prior to exposure to UV light, is very small (<8%). This can be attributed to the repulsion between the ZnO nanopowder and MB as both are positively charged at neutral pH. In contrast, around 80% of the dye is adsorbed onto the surface of the ZnO/Fe<sub>3</sub>O<sub>4</sub>/SiO<sub>2</sub> microbeads. Since the beads are comprised of 75% by mass negatively charged silica nanoparticles, the positively charged dye molecules are attracted and adsorbed on the microbeads. The negative charge of the ZnO/Fe<sub>3</sub>O<sub>4</sub>/SiO<sub>2</sub> microbeads was confirmed by measuring their zeta potential at neutral pH, which was found to be  $-18.4 \pm 0.6 \text{ mV}$  for the microbeads without Span 80 and  $-17.4 \pm 0.2 \text{ mV}$  for the microbeads with 1 wt% of Span 80. The zeta potential values are presented as mean  $\pm$  standard deviation. It is worth mentioning that the pH does not change from neutral during the course of the reaction. Fig. 8 shows that the initial dye concentration has a significant impact on the photocatalytic degradation of MB. It can be seen that the rate of degradation

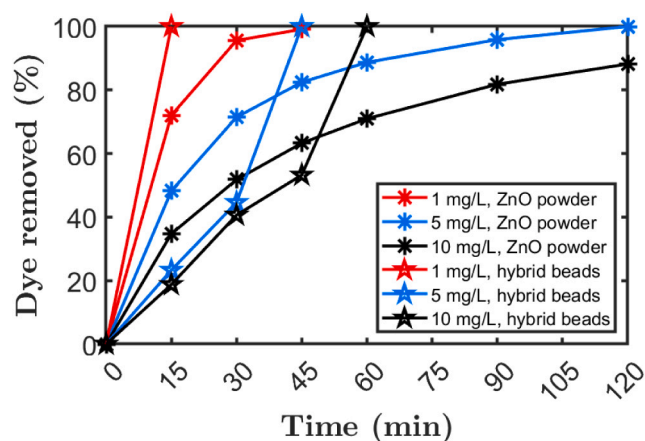


Fig. 8. The effect of initial MB concentration on its photocatalytic degradation using a fixed dosage of the photocatalyst, i.e. 2.5 mg of ZnO powder or its equivalent of 20 mg of the ZnO/Fe<sub>3</sub>O<sub>4</sub>/SiO<sub>2</sub> hybrid beads. The beads were prepared without Span 80. Each data point corresponds to a single measurement.

increases with a decrease in the initial MB concentration at the same dosage of catalyst (ZnO powder and ZnO/Fe<sub>3</sub>O<sub>4</sub>/SiO<sub>2</sub> microbeads). The rate of removal is the fastest for the lowest initial concentration of MB (i.e.  $1 \text{ mg L}^{-1}$ ). Complete removal of MB was observed within 45 and 120 min for 1 and  $5 \text{ mg L}^{-1}$ , respectively, using the ZnO nanopowder. In the case of microbeads containing the same amount of ZnO powder, complete removal of MB was observed within 15, 45 and 60 min for 1, 5 and  $10 \text{ mg L}^{-1}$ , respectively. The beads performed better compared to the ZnO powder at the same initial concentration of MB.

Jang et al. [62] and Balcha et al. [22] reported similar results for the degradation of MB using ZnO catalysts. Their studies showed that degradation decreased with an increase in the initial concentration. The increase in the concentration of MB results in higher adsorption of the dye molecules onto the surface of ZnO, which in turn impacts the catalytic activity. Furthermore, increasing the dye concentration reduces the path length of photons entering the dye solution and results in higher absorption of UV light by dye molecules rather than ZnO catalyst, which in turn decreases the catalytic efficiency [22].

### 3.3.2. Effect of catalyst dosage

Fig. 9 shows that the catalyst dosage has an effect on the removal of MB. The photocatalytic degradation results show that the highest dosage of the ZnO powder (5 mg) has a slightly higher dye removal in comparison with the other dosages of 2.5 and 3.75 mg. The dosage of ZnO powder was increased to 7.5 mg (Fig. A.14) to investigate whether a further increase has an impact. Fig. A.14 shows that the same amount of removal was observed for both catalyst dosages of 5 and 7.5 mg. This might be due to saturation of the ZnO surface with the adsorbed MB molecules, which hinders the photocatalytic process. The impact of the catalyst dosage on the photocatalytic degradation of MB is more evident for the microbeads compared to the ZnO powder at the same initial MB concentration of  $10 \text{ mg L}^{-1}$ . It can be observed that an increase in the amount of catalyst results in an increase in degradation. This can likely be attributed to the availability of more active sites. Furthermore, Fig. 9 shows that complete removal of MB was achieved using the microbeads.

### 3.3.3. Effect of bead porosity

The ZnO/Fe<sub>3</sub>O<sub>4</sub>/SiO<sub>2</sub> beads were modified to be more porous through the addition of 1 wt% of Span 80 in the oil phase during preparation. The degradation results (Fig. 10) reveal that the bead porosity has an impact at the lower dosage catalyst of 20 mg where the beads with 1 wt% of Span 80 have a higher removal rate. In addition, complete degradation of MB was obtained within 60 min for both types

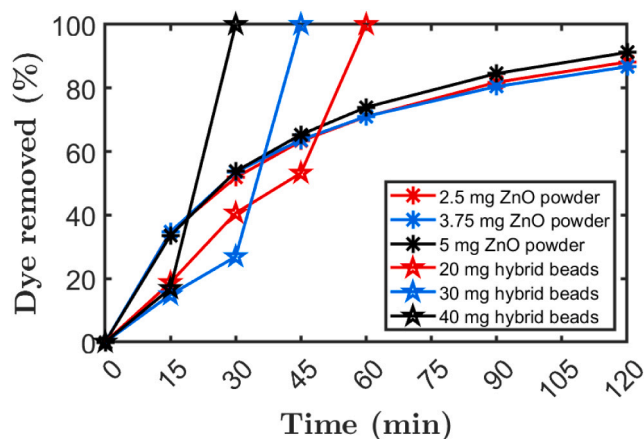


Fig. 9. The effect of catalyst dosage on the photocatalytic degradation of MB at the same initial concentration of MB solution ( $10\text{ mg L}^{-1}$ ). The beads were prepared in the absence of Span 80. Each data point corresponds to a single measurement.

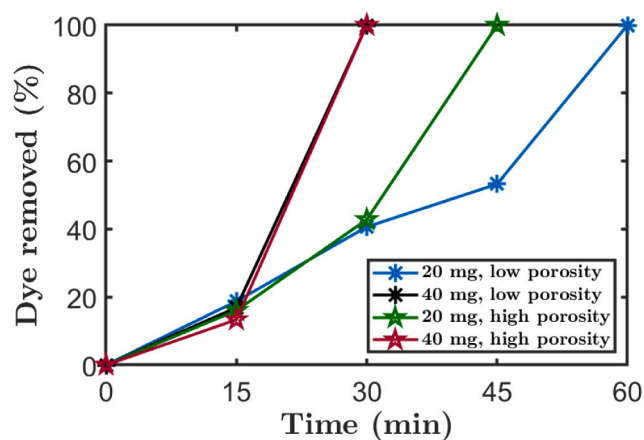


Fig. 10. The effect of bead porosity on the photocatalytic degradation of MB with an initial concentration of  $10\text{ mg L}^{-1}$ . Low porosity refers to the beads prepared without Span 80, whereas high porosity refers to beads prepared with Span 80 (1 wt%). Each data point corresponds to a single measurement.

of bead (with and without Span 80) and catalyst dosages. Brossault et al. [51] observed that the degradation of Rhodamine B was enhanced by modifying the porosity of the  $\text{TiO}_2/\text{Fe}_3\text{O}_4/\text{SiO}_2$  microbeads.

### 3.4. Magnetic response and reusability

The recovery of magnetic nanocomposites using an external magnetic field has been demonstrated for a number of systems, such as  $\text{TiO}_2\text{-SiO}_2/\text{CoFe}_2\text{O}_4$  nanocomposites [46],  $\text{ZnO}/\text{Fe}_3\text{O}_4$  nanocomposites [48–50,64],  $\text{Fe}_3\text{O}_4/\text{SiO}_2$  microbeads [56] and  $\text{TiO}_2/\text{Fe}_3\text{O}_4/\text{SiO}_2$  microbeads [51]. The response of the  $\text{ZnO}/\text{Fe}_3\text{O}_4/\text{SiO}_2$  beads to an external magnetic field was tested by placing a magnet in contact with a 5 mL aqueous suspension of beads, as illustrated in Fig. 11. It can be seen that the beads are recovered within a few seconds. The attraction of the beads to the magnet confirms the presence of  $\text{Fe}_3\text{O}_4$  nanoparticles within the beads.

The reusability of the  $\text{ZnO}/\text{Fe}_3\text{O}_4/\text{SiO}_2$  beads was investigated by using the magnetically recovered beads for two further cycles of photocatalytic degradation of MB at the same catalyst dosage (40 mg) and initial concentration of MB ( $10\text{ mg L}^{-1}$ ). It can be seen from Fig. 12 that the adsorption slightly decreases from the first cycle. The recovered beads were used immediately after the magnetic separation from the treated MB solution without washing, and therefore it is likely that

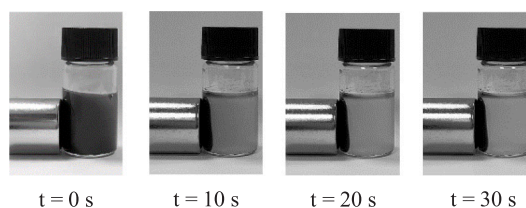


Fig. 11. The response of the  $\text{ZnO}/\text{Fe}_3\text{O}_4/\text{SiO}_2$  beads to an external magnetic field at different times. This was tested by placing a magnet in contact with a 5 mL aqueous suspension of beads prepared without Span 80. A video of the magnetic response is provided in Appendix B.

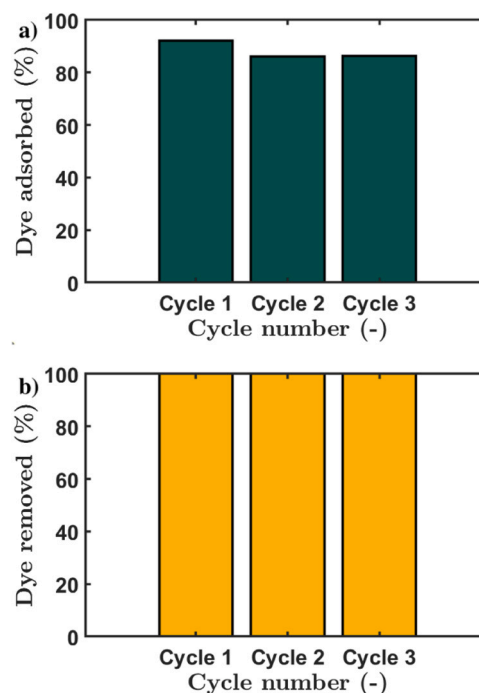


Fig. 12. Investigation of the recyclability of beads. (a) adsorption of MB on the surface of the photocatalyst and (b) the photocatalytic degradation of MB using a catalyst dosage of 40 mg and initial concentration of MB solution of  $10\text{ mg L}^{-1}$ . The beads were prepared with Span 80 (1 wt%).

residual MB was trapped on the surface of the beads. The photocatalytic degradation results in Fig. 12 show that the recycled beads were still capable of completely degrading MB. It was found that complete degradation of MB was achieved within 30 min of exposure to UV light. The results also show that the photocatalytic efficiency of the microbeads is not affected using the magnetically recovered beads as complete degradation is achieved in the two subsequent cycles using the same beads. This suggests that the  $\text{ZnO}$  within the  $\text{ZnO}/\text{Fe}_3\text{O}_4/\text{SiO}_2$  beads does not undergo photo-corrosion in these conditions.

## 4. Conclusions

A photocatalyst in the form of  $\text{ZnO}/\text{Fe}_3\text{O}_4/\text{SiO}_2$  microbeads was prepared through the salt-induced destabilisation and subsequent agglomeration of nanoparticles in a W/O emulsion template. The work shows the potential of such system for the removal of cationic azo dyes from wastewater through photocatalytic degradation. The catalyst dosage, initial concentration of MB solution and the porosity of beads have an impact on the degradation process of MB. Since the beads are magnetically separable due to the presence of the magnetic nanoparticles, it was possible to recover the beads and use them for further degradation experiments. The strong attraction between the

negatively charged beads and positively charged MB molecules results in higher adsorption and photocatalytic degradation of MB in comparison with the ZnO powder at the same conditions. This work shows that complete degradation can be achieved using small amounts of the ZnO/Fe<sub>3</sub>O<sub>4</sub>/SiO<sub>2</sub> microbeads upon exposure to low-power UV-light.

#### CRediT authorship contribution statement

**Mohammed Al-Sharabi:** Writing – review & editing, Writing – original draft, Visualization, Methodology, Investigation, Formal analysis, Data curation, Conceptualization. **Daniele Baiocco:** Writing – review & editing, Investigation. **Benjamin T. Lobel:** Writing – review & editing, Investigation. **Olivier J. Cayre:** Writing – review & editing, Supervision, Resources, Project administration, Investigation, Funding acquisition, Conceptualization. **Zhibing Zhang:** Writing – review & editing, Supervision, Resources, Project administration, Investigation, Funding acquisition and Conceptualization. **Alexander F. Routh:** Writing – review & editing, Supervision, Resources, Project administration, Investigation, Funding acquisition, Conceptualization.

#### Declaration of competing interest

The authors declare that they have no known competing financial interests or personal relationships that could have appeared to influence the work reported in this paper.

#### Data availability

Data will be made available on request.

#### Acknowledgements

The authors would like to thank the U.K. Engineering and Physical Sciences Research Council (EPSRC) for their funding (EP/V027727/1, EP/V027646/1, and EP/V027654/1). The authors would also like to thank the EPSRC Underpinning Multi-User Equipment Call (EP/P030467/1) for funding the TEM. Dr. Heather Greer from the Department of Chemistry at the University of Cambridge is also thanked for assisting with the SEM, TEM and STEM imaging and EDX analysis.

#### Appendix A

##### A.1. Adsorption isotherm

The surface specific mass of MB adsorbed onto the silica nanoparticles was calculated using Eq. (A.1).

$$m = \frac{V(C_0 - C_t)}{A} \quad (\text{A.1})$$

where  $m$  is the mass of adsorbed MB (mg/m<sup>2</sup> silica),  $V$  is the volume of MB solution (L),  $C_0$  is the initial concentration of MB before adsorption (mg/L),  $C_t$  is the concentration of MB after adsorption (mg/L) and  $A$  is the surface area of silica (m<sup>2</sup>).

##### A.2. UV-Vis analysis

See Fig. A.13.

##### A.3. Effect of catalyst dosage

See Fig. A.14.

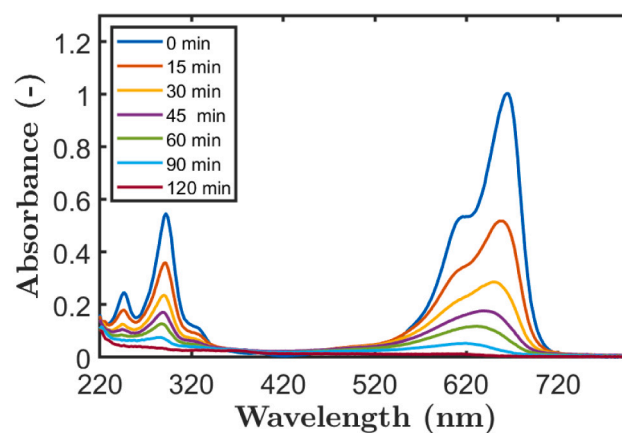


Fig. A.13. The UV-Vis absorption spectra of the photocatalytic degradation of a MB solution with an initial dye concentration of 5 mg L<sup>-1</sup> by ZnO powder (2.5 mg) in the range of 220 to 800 nm. Time was measured from the start of the photocatalytic degradation process.

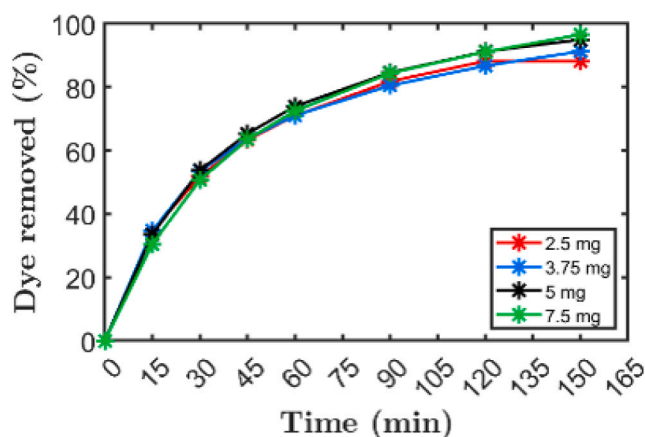


Fig. A.14. The effect of catalyst dosage in the form of ZnO powder on the photocatalytic degradation of MB at the same initial concentration of MB solution (10 mg L<sup>-1</sup>).

#### Appendix B. Supplementary data

Supplementary material related to this article can be found online at <https://doi.org/10.1016/j.colsurfa.2024.134169>.

#### References

- [1] M. Vidal, R. Garcia-Arrona, A. Bordagaray, M. Ostra, G. Albizu, Simultaneous determination of color additives tartrazine and allura red in food products by digital image analysis, *Talanta* 184 (2018) 58–64.
- [2] M. Leulescu, A. Rotaru, A. Moanță, G. Iacobescu, I. Pălărie, N. Cioateră, M. Popescu, M.C. Criveanu, E. Morintale, M. Bojan, P. Rotaru, Azorubine: physical, thermal and bioactive properties of the widely employed food, pharmaceutical and cosmetic red azo dye material, *J. Therm. Anal. Calorim.* 143 (2021) 3945–3967.
- [3] V. Selvaraj, T.S. Karthika, C. Mansiya, M. Alagar, An over review on recently developed techniques, mechanisms and intermediate involved in the advanced azo dye degradation for industrial applications, *J. Mol. Struct.* 1224 (2021) 129195.
- [4] K. Yamjala, M.S. Nainar, N.R. Ramiseti, Methods for the analysis of azo dyes employed in food industry – A review, *Food Chem.* 192 (2016) 813–824.
- [5] Y.-L. Oon, S.-A. Ong, L.-N. Ho, Y.-S. Wong, F.A. Dahalan, Y.-S. Oon, T.-P. Teoh, H.-K. Lehl, W.-E. Thung, Constructed wetland-microbial fuel cell for azo dyes degradation and energy recovery: Influence of molecular structure, kinetics, mechanisms and degradation pathways, *Sci. Total Environ.* 720 (2020) 137370.
- [6] Y. Shi, Z. Yang, L. Xing, X. Zhang, X. Li, D. Zhang, Recent advances in the biodegradation of azo dyes, *World J. Microbiol. Biotechnol.* 37 (2021) 1–18.

- [7] A. Sahoo, S. Patra, A combined process for the degradation of azo-dyes and efficient removal of aromatic amines using porous silicon supported porous ruthenium nanocatalyst, *ACS Appl. Nano Mater.* 1 (9) (2018) 5169–5178.
- [8] S.R. Geed, K. Samal, A. Tagade, Development of adsorption-biodegradation hybrid process for removal of methylene blue from wastewater, *J. Environ. Chem. Eng.* 7 (6) (2019) 103439.
- [9] L.F. Cusioli, H.B. Quesada, A.T.A. Baptista, R.G. Gomes, R. Bergamasco, Soybean hulls as a low-cost biosorbent for removal of methylene blue contaminant, *Environ. Prog. Sustain. Energy* (2020).
- [10] T.A. Kurniawan, Z. Mengting, D. Fu, S.K. Yeap, M.H.D. Othman, R. Avtar, T. Ouyang, Functionalizing TiO<sub>2</sub> with graphene oxide for enhancing photocatalytic degradation of methylene blue (MB) in contaminated wastewater, *J. Environ. Manag.* 270 (2020) 110871.
- [11] T.Q.Q. Viet, V.H. Khoi, N.T.H. Giang, H.T.V. Hoang Anh, N.M. Dat, M.T. Phong, N.H. Hieu, Statistical screening and optimization of photocatalytic degradation of methylene blue by ZnO–TiO<sub>2</sub>/rGO nanocomposite, *Colloids Surf. A* 629 (2021) 127464.
- [12] F. Temel, M. Turkyilmaz, S. Kucukcongar, Removal of methylene blue from aqueous solutions by silica gel supported calix[4]arene cage: Investigation of adsorption properties, *Eur. Polym. J.* 125 (2020) 109540.
- [13] S. Xia, L. Zhang, G. Pan, P. Qian, Z. Ni, Photocatalytic degradation of methylene blue with a nanocomposite system: synthesis, photocatalysis and degradation pathways, *Phys. Chem. Chem. Phys.* 17 (2015) 5345–5351.
- [14] H. Dong, T. Guo, W. Zhang, H. Ying, P. Wang, Y. Wang, Y. Chen, Biochemical characterization of a novel azoreductase from *Streptomyces* sp.: Application in eco-friendly decolorization of azo dye wastewater, *Int. J. Biol. Macromol.* 140 (2019) 1037–1046.
- [15] Q. Li, Y. Li, X. Ma, Q. Du, K. Sui, D. Wang, C. Wang, H. Li, Y. Xia, Filtration and adsorption properties of porous calcium alginate membrane for methylene blue removal from water, *Chem. Eng. J.* 316 (2017) 623–630.
- [16] M.-C. Rosu, M. Coros, F. Pogacean, L. Magerusan, C. Socaci, A. Turza, S. Pruneanu, Azo dyes degradation using TiO<sub>2</sub>-Pt/graphene oxide and TiO<sub>2</sub>-Pt/reduced graphene oxide photocatalysts under UV and natural sunlight irradiation, *Solid State Sci.* 70 (2017) 13–20.
- [17] V. Innocenzi, M. Prisciandaro, M. Centofanti, F. Vegliò, Comparison of performances of hydrodynamic cavitation in combined treatments based on hybrid induced advanced fenton process for degradation of azo-dyes, *J. Environ. Chem. Eng.* 7 (3) (2019) 103171.
- [18] W. Song, J. Li, X. Zhang, J. Feng, X. Du, Q. Wang, C. Fu, W. Qiu, Z. Wang, X. Gao, A feasible approach for azo-dye methyl orange degradation in siderite/H<sub>2</sub>O<sub>2</sub> assisted by persulfate: Optimization using response surface methodology and pathway, *J. Environ. Manag.* 308 (2022) 114397.
- [19] X. Chen, Z. Wu, D. Liu, Z. Gao, Preparation of ZnO photocatalyst for the efficient and rapid photocatalytic degradation of azo dyes, *Nanoscale Res. Lett.* 12 (2017) 1–10.
- [20] C.H. Kwon, H. Shin, J.H. Kim, W.S. Choi, K.H. Yoon, Degradation of methylene blue via photocatalysis of titanium dioxide, *Mater. Chem. Phys.* 86 (1) (2004) 78–82.
- [21] C. Xu, G.P. Rangaiah, X.S. Zhao, Photocatalytic degradation of methylene blue by titanium dioxide: Experimental and modeling study, *Ind. Eng. Chem. Res.* 53 (38) (2014) 14641–14649.
- [22] A. Balcha, O.P. Yadav, T. Dey, Photocatalytic degradation of methylene blue dye by zinc oxide nanoparticles obtained from precipitation and sol-gel methods, *Environ. Sci. Pollut. Res.* 23 (2016) 25485–25493.
- [23] P.A. Luque, C.A. Soto-Robles, O. Nava, C.M. Gomez-Gutierrez, A. Castro-Beltran, H.E. Garrafa-Galvez, A.R. Vilchis-Nestor, A. Olivas, Green synthesis of zinc oxide nanoparticles using *Citrus sinensis* extract, *J. Mater. Sci., Mater. Electron.* 29 (2018) 9764–9770.
- [24] L. Chen, I. Batjikh, J. Hurl, Y. Han, Y. Huo, H. Ali, J.F. Li, E.J. Rupa, J.c. Ahn, R. Mathiyalagan, D.C. Yang, Green synthesis of zinc oxide nanoparticles from root extract of *Scutellaria baicalensis* and its photocatalytic degradation activity using methylene blue, *Optik* 184 (2019) 324–329.
- [25] D.A. Bopape, D.E. Motaung, N.C. Hintsho-Mbita, Green synthesis of ZnO: Effect of plant concentration on the morphology, optical properties and photodegradation of dyes and antibiotics in wastewater, *Optik* 251 (2022) 168459.
- [26] G. Elango, S.M. Roopan, Efficacy of SnO<sub>2</sub> nanoparticles toward photocatalytic degradation of methylene blue dye, *J. Photochem. Photobiol. B: Biol.* 155 (2016) 34–38.
- [27] S.P. Kim, M.Y. Choi, H.C. Choi, Photocatalytic activity of SnO<sub>2</sub> nanoparticles in methylene blue degradation, *Mater. Res. Bull.* 74 (2016) 85–89.
- [28] M. Arakha, J. Roy, P.S. Nayak, B. Mallick, J. S., Zinc oxide nanoparticle energy band gap reduction triggers the oxidative stress resulting into autophagy-mediated apoptotic cell death, *Free Radic. Biol. Med.* 110 (2017) 42–53.
- [29] R. Raliya, C. Avery, S. Chakrabarti, P. Biswas, Photocatalytic degradation of methyl orange dye by pristine titanium dioxide, zinc oxide, and graphene oxide nanostructures and their composites under visible light irradiation, *Appl. Nanosci.* 7 (2017) 253–259.
- [30] H. Liang, X. Tai, Z. Du, Y. Yin, Enhanced photocatalytic activity of ZnO sensitized by carbon quantum dots and application in phenol wastewater, *Opt. Mater.* 100 (2020) 109674.
- [31] K.M. Lee, C.W. Lai, K.S. Ngai, J.C. Juan, Recent developments of zinc oxide based photocatalyst in water treatment technology: A review, *Water Res.* 88 (2016) 428–448.
- [32] P. Franco, O. Sacco, I. De Marco, V. Vaiano, Zinc oxide nanoparticles obtained by supercritical antisolvent precipitation for the photocatalytic degradation of crystal violet dye, *Catalysts* 9 (4) (2019).
- [33] T. Sansenya, N. Masri, T. Chankhanitha, T. Senasu, J. Piriyanon, S. Mukdasai, S. Nanan, Hydrothermal synthesis of ZnO photocatalyst for detoxification of anionic azo dyes and antibiotic, *J. Phys. Chem. Solids* 160 (2022) 110353.
- [34] Y. Li, K. Liu, J. Zhang, J. Yang, Y. Huang, Y. Tong, Engineering the band-edge of Fe<sub>2</sub>O<sub>3</sub>/ZnO nanoplates via separate dual cation incorporation for efficient photocatalytic performance, *Ind. Eng. Chem. Res.* 59 (42) (2020) 18865–18872.
- [35] K. Liu, D. Chen, S. Zhang, P. Su, Y. Huang, Enhancing the charge carrier transfer of ZnFe<sub>2</sub>O<sub>4</sub>/C/TiO<sub>2</sub> hollow nanosphere photocatalyst via contact interface engineering, *Ind. Eng. Chem. Res.* 60 (35) (2021) 12893–12900.
- [36] T. Nam Anh, N. Thi Hien, V. Tan Tran, D. Thi Hai Linh, N. Thi Hanh, L. Thi Do, N. Hung Vu, N. Minh Hoang, D. Viet Quang, V.-D. Dao, 92.58 Solution by Pt/WO<sub>3</sub> nanohybrid, *Inorg. Chem. Commun.* 161 (2024) 112100.
- [37] M. Alomar, S. Alterary, M. Awad, I. Ahmed, A. Danish, M.S. Irshad, B. Thi My Duyen, T.A. Anh, V.-D. Dao, Morphological regulation of CdS/Ga<sub>0.04</sub>Cd<sub>0.96</sub>S nanocomposites for enhanced efficiency of solar-driven rhodamine B degradation, *J. Alloys Compd.* 980 (2024) 173506.
- [38] V. Vaiano, G. Iervolino, Photocatalytic removal of methyl orange azo dye with simultaneous hydrogen production using Ru-modified ZnO photocatalyst, *Catalysts* 9 (11) (2019).
- [39] M. Maruthupandy, P. Qin, T. Muneeswaran, G. Rajivgandhi, F. Quero, J.-M. Song, Graphene-zinc oxide nanocomposites (G-ZnO NCs): Synthesis, characterization and their photocatalytic degradation of dye molecules, *Mater. Sci. Eng. B* 254 (2020) 114516.
- [40] A. Syampurwadi, I. Primadona, V. Fauzia, Facile photochemical reduction synthesis of bimetallic Au and Pd nanoparticles on ZnO nanorods for improved photocatalytic degradation of methylene blue, *Adv. Natl. Sci.: Nanosci. Nanotechnol.* 13 (2) (2022) 025013.
- [41] R. Atchudan, T.N.J.I. Edison, S. Perumal, D. Karthikeyan, Y.R. Lee, Facile synthesis of zinc oxide nanoparticles decorated graphene oxide composite via simple solvothermal route and their photocatalytic activity on methylene blue degradation, *J. Photochem. Photobiol. B: Biol.* 162 (2016) 500–510.
- [42] L. Zhang, L. Du, X. Cai, X. Yu, D. Zhang, L. Liang, P. Yang, X. Xing, W. Mai, S. Tan, Y. Gu, J. Song, Role of graphene in great enhancement of photocatalytic activity of ZnO nanoparticle–graphene hybrids, *Physica E* 47 (2013) 279–284.
- [43] N. Raghavan, S. Thangavel, G. Venugopal, Enhanced photocatalytic degradation of methylene blue by reduced graphene-oxide/titanium dioxide/zinc oxide ternary nanocomposites, *Mater. Sci. Semicond. Process.* 30 (2015) 321–329.
- [44] N.T. Padmanabhan, N. Thomas, J. Louis, D.T. Mathew, P. Ganguly, H. John, S.C. Pillai, Graphene coupled TiO<sub>2</sub> photocatalysts for environmental applications: A review, *Chemosphere* 271 (2021) 129506.
- [45] Q. Feng, S. Li, W. Ma, H.-J. Fan, X. Wan, Y. Lei, Z. Chen, J. Yang, B. Qin, Synthesis and characterization of Fe<sub>3</sub>O<sub>4</sub>/ZnO-GO nanocomposites with improved photocatalytic degradation methyl orange under visible light irradiation, *J. Alloys Compd.* 737 (2018) 197–206.
- [46] F.A. Harraz, R.M. Mohamed, M.M. Rashad, Y.C. Wang, W. Sigmund, Magnetic nanocomposite based on titania–silica/cobalt ferrite for photocatalytic degradation of methylene blue dye, *Ceram. Int.* 40 (1, Part A) (2014) 375–384.
- [47] M. Yilmaz, N. Mengelizadeh, M. Saloot, S. shahbaksh, D. Balarak, Facile synthesis of Fe<sub>3</sub>O<sub>4</sub>/ZnO/GO photocatalysts for decolorization of acid blue 113 under solar, visible and UV lights, *Mater. Sci. Semicond. Process.* 144 (2022) 106593.
- [48] P. Thi Lan Huong, N. Van Quang, N. Thi Huyen, H. Thu Huong, D. Anh Tuan, M. Trung Tran, Q. Vinh Tran, T. Ngoc Bach, N. Tu, V.-D. Dao, Efficiency enhancement of photocatalytic activity under UV and visible light irradiation using ZnO/Fe<sub>3</sub>O<sub>4</sub> heterostructures, *Sol. Energy* 249 (2023) 712–724.
- [49] C. Karunakaran, P. Vinayagamorthy, J. Jayabharathi, Nonquenching of charge carriers by Fe<sub>3</sub>O<sub>4</sub> core in Fe<sub>3</sub>O<sub>4</sub>/ZnO nanosheet photocatalyst, *Langmuir* 30 (49) (2014) 15031–15039.
- [50] M. Akkari, P. Aranda, A. Mayoral, M. García-Hernández, A. Ben Haj Amara, E. Ruiz-Hitzky, Sepiolite nanoplateform for the simultaneous assembly of magnetite and zinc oxide nanoparticles as photocatalyst for improving removal of organic pollutants, *J. Hazard. Mater.* 340 (2017) 281–290.
- [51] D.F.F. Brossault, T.M. McCoy, A.F. Routh, Self-assembly of TiO<sub>2</sub>/Fe<sub>3</sub>O<sub>4</sub>/SiO<sub>2</sub> microbeads: A green approach to produce magnetic photocatalysts, *J. Colloid Interface Sci.* 584 (2021) 779–788.
- [52] T. Mao, M. Liu, L. Lin, Y. Cheng, C. Fang, A study on doping and compound of Zinc Oxide photocatalysts, *Polymers* 14 (21) (2022).
- [53] K.P. Gopinath, N.V. Madhav, A. Krishnan, R. Malolan, G. Rangarajan, Present applications of titanium dioxide for the photocatalytic removal of pollutants from water: A review, *J. Environ. Manag.* 270 (2020) 110906.
- [54] R.H. Waghchaure, V.A. Adole, B.S. Jagdale, Photocatalytic degradation of methylene blue, rhodamine B, methyl orange and Eriochrome black T dyes by modified ZnO nanocatalysts: A concise review, *Inorg. Chem. Commun.* 143 (2022) 109764.

- [55] S. Hernández, D. Hidalgo, A. Sacco, A. Chiodoni, A. Lamberti, V. Cauda, E. Tresso, G. Saracco, Comparison of photocatalytic and transport properties of TiO<sub>2</sub> and ZnO nanostructures for solar-driven water splitting, *Phys. Chem. Chem. Phys.* 17 (2015) 7775–7786.
- [56] D.F.F. Brossault, A.F. Routh, Salt-driven assembly of magnetic silica microbeads with tunable porosity, *J. Colloid Interface Sci.* 562 (2020) 381–390.
- [57] J. Lu, I. Batjikh, J. Hurh, Y. Han, H. Ali, R. Mathiyalagan, C. Ling, J.C. Ahn, D.C. Yang, Photocatalytic degradation of methylene blue using biosynthesized zinc oxide nanoparticles from bark extract of *Kalopanax septemlobus*, *Optik* 182 (2019) 980–985.
- [58] V.-P. Dinh, T.-D.-T. Huynh, H.M. Le, V.-D. Nguyen, V.-A. Dao, N.Q. Hung, L.A. Tuyen, S. Lee, J. Yi, T.D. Nguyen, L.V. Tan, Insight into the adsorption mechanisms of methylene blue and chromium(iii) from aqueous solution onto pomelo fruit peel, *RSC Adv.* 9 (2019) 25847–25860.
- [59] M. Ramesh, M. Anbuvaran, G. Viruthagiri, Green synthesis of ZnO nanoparticles using *Solanum nigrum* leaf extract and their antibacterial activity, *Spectrochimica Acta A* 136 (2015) 864–870.
- [60] P. Kumar, A. Kumar, M.A. Rizvi, S.K. Moosvi, V. Krishnan, M.M. Duvenhage, W.D. Roos, H.C. Swart, Surface, optical and photocatalytic properties of rb doped ZnO nanoparticles, *Appl. Surf. Sci.* 514 (2020) 145930.
- [61] C.B. Ong, L.Y. Ng, A.W. Mohammad, A review of ZnO nanoparticles as solar photocatalysts: Synthesis, mechanisms and applications, *Renew. Sustain. Energy Rev.* 81 (2018) 536–551.
- [62] Y.J. Jang, C. Simer, T. Ohm, Comparison of zinc oxide nanoparticles and its nano-crystalline particles on the photocatalytic degradation of methylene blue, *Mater. Res. Bull.* 41 (1) (2006) 67–77.
- [63] X. Yu, L. Huang, Y. Wei, J. Zhang, Z. Zhao, W. Dai, B. Yao, Controllable preparation, characterization and performance of Cu<sub>2</sub>O thin film and photocatalytic degradation of methylene blue using response surface methodology, *Mater. Res. Bull.* 64 (2015) 410–417.
- [64] H.L. Pham, V.D. Nguyen, V.K. Nguyen, T.H.P. Le, N.B. Ta, D.C. Pham, Q.T. Tran, V.T. Dang, Rational design of magnetically separable core/shell Fe<sub>3</sub>O<sub>4</sub>/ZnO heterostructures for enhanced visible-light photodegradation performance, *RSC Adv.* 11 (2021) 22317–22326.